

Empirics of multi-modal traffic networks

Using the 3D macroscopic fundamental diagram

Journal Article

Author(s):

Loder, Allister; Ambühl, Lukas; Menendez, Monica; Axhausen, Kay W. 

Publication date:

2017-09

Permanent link:

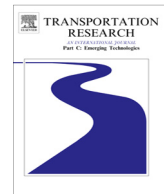
<https://doi.org/10.3929/ethz-b-000166603>

Rights / license:

[Creative Commons Attribution-NonCommercial-NoDerivatives 4.0 International](#)

Originally published in:

Transportation Research Part C: Emerging Technologies 82, <https://doi.org/10.1016/j.trc.2017.06.009>



Empirics of multi-modal traffic networks – Using the 3D macroscopic fundamental diagram



Allister Loder^a, Lukas Ambühl^{a,*}, Monica Menendez^a, Kay W. Axhausen^a

^a Institute for Transport Planning and Systems, ETH Zurich, Switzerland

ARTICLE INFO

Article history:

Received 16 December 2016

Received in revised form 12 June 2017

Accepted 13 June 2017

Available online 26 June 2017

Keywords:

Macroscopic fundamental diagram

Multi-modal traffic

Public transport

Urban traffic

Mode share

ABSTRACT

Traffic is multi-modal in most cities. However, the impacts of different transport modes on traffic performance and on each other are unclear – especially at the network level. The recent extension of the macroscopic fundamental diagram (MFD) into the 3D-MFD offers a novel framework to address this gap at the urban scale. The 3D-MFD relates the network accumulation of cars and public transport vehicles to the network travel production, for either vehicles or passengers. No empirical 3D-MFD has been reported so far.

In this paper, we present the first empirical estimate of a 3D-MFD at the urban scale. To this end, we use data from loop detectors and automatic vehicle location devices (AVL) of the public transport vehicles in the city of Zurich, Switzerland. We compare two different areas within the city, that differ in their topology and share of dedicated lanes for public transport. We propose a statistical model of the 3D-MFD, which estimates the effects of the vehicle accumulation on car and public transport speeds under multi-modal traffic conditions. The results quantify the effects of both, vehicles and passengers, and confirm that a greater share of dedicated lanes reduces the marginal effects of public transport vehicles on car speeds. Lastly, we derive a new application of the 3D-MFD by identifying the share of public transport users that maximizes the journey speeds in an urban network accounting for all motorized transport modes.

© 2017 The Authors. Published by Elsevier Ltd. This is an open access article under the CC BY-NC-ND license (<http://creativecommons.org/licenses/by-nc-nd/4.0/>).

1. Introduction and background

Potential benefits from public transport provision and improvements in urban transportation networks are not limited to reduction in passengers travel time (Hensher, 2001) or congestion relief (Adler and van Ommeren, 2016; Anderson, 2014), but also include an increase in agglomeration economies (Chatman and Noland, 2011). The literature is abundant regarding the share of public transport users (from the set of all users) that maximizes these benefits (Small and Verhoef, 2007; Tirachini and Hensher, 2012). While infrastructure investments for both modes are long-term-oriented, an optimal modal share of public transport users for the short term considers how travel demand should be allocated to existing infrastructure while improving accessibility for all users. Recent advances in understanding network-wide traffic through the macroscopic fundamental diagram (MFD), a well-defined and reproducible relationship between vehicle network accumulation and network production (Geroliminis and Daganzo, 2008), offer a new approach for optimal demand allocation to existing infrastructure. The MFD is considered invariant to small changes in demand, so network topology in combination with traffic control determine its shape (Daganzo and Geroliminis, 2008). Public transport and private cars do not affect congestion

* Corresponding author.

E-mail address: lukas.ambuehl@iwt.baug.ethz.ch (L. Ambühl).

equally (Boyaci and Geroliminis, 2011; Chiabaut et al., 2014; Gronau, 2000). To properly account for these two systems, the MFD must be extended to the multi-modal or 3D-MFD (Geroliminis et al., 2014), that integrates transport modes. Although promising, no empirical 3D-MFD has yet been reported. Such empirical study, however, is crucial for further applications of the 3D-MFD in transportation and economics.

In this paper, we present the first empirical estimate of a 3D-MFD at the urban scale, using data from loop detectors and automatic vehicle location devices (AVL) for the city of Zurich, Switzerland. We combine both vehicle and passenger data to statistically estimate the multi-modal interaction effects at vehicle and passenger levels. We compare such interaction effects for two regions in the city of Zurich differing in their share of dedicated lanes for public transport. We find evidence that cars and public transport vehicles do not contribute equally to congestion and that a greater share of dedicated lanes reduces multi-modal interaction effects. Finally, we derive a new application of the 3D-MFD by linking the share of public transport users to the average journey speeds in the city. Using this approach, we then identify the optimal share of public transport users that maximizes journey speeds in an urban area (considering all motorized transport modes).

In the following, we give a literature overview. First, we concentrate on the car MFD, then on the interactions between cars and public transport at a network level, from both vehicle and passenger perspectives, including the concept of the 3D-MFD.

Origins of the MFD can be traced back to network traffic flow theory in the 1960s and are based on work by Godfrey (1969), Herman and Prigogine (1979), Smeed (1961, 1968), Thomson (1967) and Wardrop (1968). In the 1980s, Mahmassani et al. (1984, 1987) and Williams et al. (1987) used simulations to relate average speed, flow and density at the network level. The studies found that the network relationships of these variables are similar to their link-based counterparts. The concept of the macroscopic traffic flow analysis was then re-initiated by Daganzo (2007). Daganzo and Geroliminis (2008) used variational theory to analytically derive the MFD as a characteristic of a network (free flow speed, average link length, link capacity, traffic signal cycle characteristics, jam density, and backward wave speed) and found it to be a well-defined and reproducible curve. Laval and Castrillón (2015) showed with a stochastic approach that the two dimensionless parameters, mean block length to green ratio and the mean red to green ratio, are the main drivers of the MFDs shape. In addition to simulation and analytical estimates of the MFD, the macroscopic relationship has also been observed using empirical data. The MFD has been shown to exist for Yokohama, Japan (Geroliminis and Daganzo, 2008), Toulouse, France (Buisson and Ladier, 2009), Brisbane, Australia (Tsubota et al., 2014), Shenzhen, China (Ji et al., 2014), Sendai, Japan (Wang et al., 2015) and Zurich, Switzerland (Ambühl et al., 2017). Such estimates are typically based on either loop detector data or floating car data, although both data sources have some drawbacks (Ambühl et al., 2017; Buisson and Ladier, 2009; Du et al., 2016), hence efforts have been made to fuse them (Ambühl and Menendez, 2016). So far, the MFD has been applied to traffic control (e.g. Aboudolas and Geroliminis, 2013; Girault et al., 2016; Haddad and Geroliminis, 2012), pricing (e.g. Zheng et al., 2012, 2016), investigation of the network topology's impact on traffic performance (e.g. Knoop et al., 2014, 2015; Muhlich et al., 2015; Ortigosa et al., 2015, 2017a) and to describe the effects of other systems, in particular parking (e.g. Cao and Menendez, 2015; Geroliminis, 2015; Leclercq et al., 2017; Zheng and Geroliminis, 2016).

Although public transport plays an important role in cities, its impact on traffic at the network level has not received much attention in literature. At the link level, analytical approaches have been developed to quantify maximum capacity of mixed traffic and analyze the effects of stop types, dwell times and distances between stops on speeds (Anderhub et al., 2008; Chiabaut, 2015; Chiabaut et al., 2014; He et al., 2017; Köhler et al., 1998; Lüthy et al., 2016) and empirical data has been used to analyze car capacity with and without buses (Arnet et al., 2015). At intersection level, existing literature on multi-modal interactions is rather large, e.g. Guler and Menendez (2014a,b), He et al. (2016) and Moghimdarzi et al. (2016) analyzed bus priority at signalized intersections and Gu et al. (2013, 2014) analyzed the effects on car traffic of bus stops close to an intersection. At the network level, Smeed (1961, 1968) discussed the effects of car and bus interactions on the respective travel times, and the effect of urban design on traffic performance, emphasizing the dilemma between public and private transport modes for both travel times and vehicle occupancies. Work following Smeed's macroscopic relations was almost non-existent for decades, until Boyaci and Geroliminis (2011) discussed urban design and multi-modal capacities at network level, Nikias et al. (2016) quantified the effects of bus operations on the traffic performance of urban networks, and Geroliminis et al. (2014) extended the MFD to a 3D-MFD using simulation data. The maximum vehicular flow in a 3D-MFD occurs when no public transport vehicles operate. When including passenger flows, the 3D-MFD becomes the 3D-passenger MFD (3D-pMFD). The maximum passenger flow in a 3D-pMFD is observed at non-zero provision of public transport. Chiabaut (2015) related the accumulation of passengers per kilometer to passenger flow and discussed the concept of the 3D-MFD for multi-modal arterials from a passenger's point of view, emphasizing the user and system optimum. While analytical approximations for MFDs concentrating on cars (Daganzo and Geroliminis, 2008; Geroliminis and Boyaci, 2012; Leclercq and Geroliminis, 2013) and multi-modal MFDs (Boyaci and Geroliminis, 2011; Chiabaut, 2015; Chiabaut et al., 2014) exist, empirical MFDs have only been obtained for cars so far. Data describing multi-modal relations has been obtained only from simulations of San Francisco and Zurich (Geroliminis et al., 2014; Menendez et al., 2016; Ortigosa et al., 2017b). First applications of the 3D-MFD (and 3D-pMFD) are related to urban space allocation (Zheng and Geroliminis, 2013), parking (Zheng and Geroliminis, 2016) and mode choice (Schreiber et al., 2016).

The remainder of this paper is organized as follows; in Section 2, we describe the case study for Zurich with the available data. In Section 3, we present the empirical 3D-MFD. In Section 4, we propose a model to quantify the effects of bi-modal traffic at the network level. In Section 5, we show the results of the proposed model for both, vehicles and passengers. In

Section 6, we present a methodology to derive the optimal share of public transport users from the 3D-MFD. We then finish in Section 7 with some concluding remarks.

2. Data

2.1. Analyzed areas and time period

Zurich is the largest city in Switzerland, encompassing an area of around 92 km², with a population of approximately 400,000 and roughly 300,000 daily inbound commuters. The road network, excluding motorways, has a length of 740 km. For the analysis reported here, we concentrate on the time period between the 26th and the 30th of October 2015 (a total of 5 weekdays). For each day, we use data from 06:00 to 24:00 (the public transport operating time). We focus on two regions within Zurich, each with an area of approximately 2 km². Fig. 1 shows both regions shaded in gray. Roads monitored by loop detectors are highlighted as thick light gray lines and the locations of the loop detectors are indicated by white dots. Public transport lines are shown in thin black lines. Note that some parts of public transport lines run completely separated from private transport. We denote the zone in the west as Wiedikon and the zone in the east as City center. The zones are selected for a couple of reasons. First, the regions differ in their share of dedicated lanes for public transport; in the City center almost 75% of the lane-km used by public transport are dedicated, whereas in Wiedikon this number is 60%. Second, we have chosen small areas in order not to violate the homogeneity assumption of the MFD. The size of the zones is about one-fourth of the one analyzed in Yokohama by Geroliminis and Daganzo (2008), and half as large or even magnitudes smaller than the regions which resulted from static and dynamic partitioning in Shenzhen (Ji et al., 2014). Third, our selected regions have a homogeneous topology and similar hierarchy in the road network, e.g. no presence of freeways. Thus, we avoid further partitioning of the network.

The overall Zurich network can be split into three parts. In the first part, only cars circulate, in the second part only public transport vehicles circulate, and in the third part both modes share the same road space. It is important to note that even when both modes share the same link they do not necessarily share the same lane. Consequently, the total network length is not simply the sum of the car network length and the public transport network length. Table 1 summarizes the transport network characteristics for both transport modes in the two regions. In the City center, the public transport network length includes 22 km for trams and 12 km for buses, while in Wiedikon, 7 km are for trams and 18 km for buses. Given that both regions have a high share of dedicated lanes for public transport, interactions between both modes occur particularly at intersections and curbside stops.

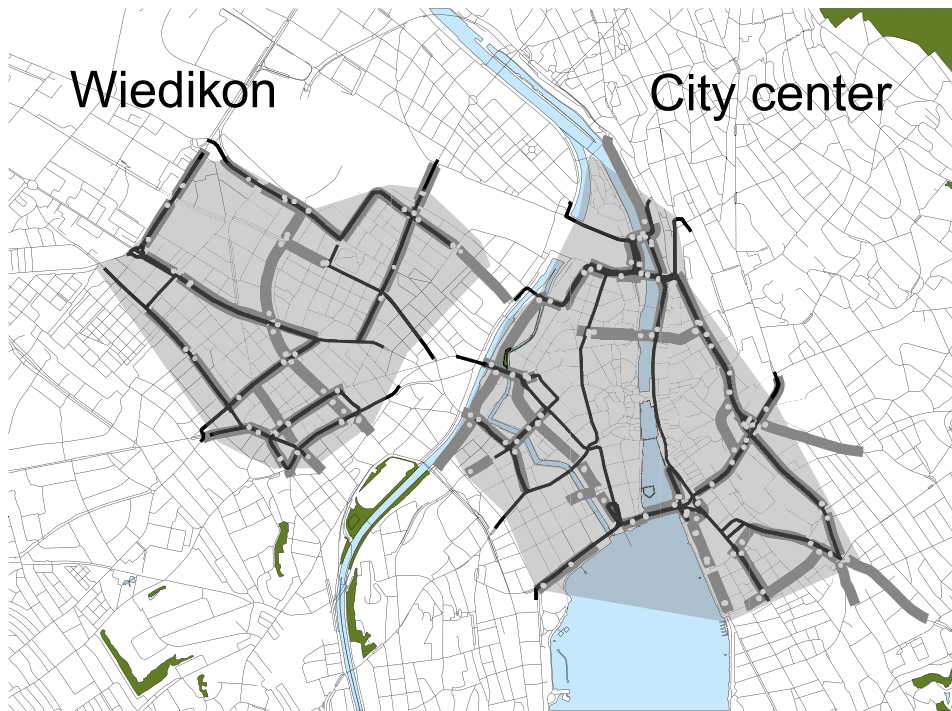


Fig. 1. Zones of analysis and the networks considered are shaded in gray. Public transport lines are marked as thin black lines. Locations of loop detectors are marked by white dots and the links they cover are emphasized as thick light gray lines. Note that the map also shows residential streets not considered in this analysis. Map reproduced with the authorization of swisstopo (JA100120). (For interpretation of the references to color in this figure legend, the reader is referred to the web version of this article.)

Table 1

Statistics of Zurich's private and public transport networks.

		City center	Wiedikon
Car network length, L_c	[lane-km]	39	31
Average link length of L_c , \bar{l}_c	[km]	0.163	0.279
L_c covered by loop detectors	[lane-km]	24	10
Number of signalized intersections		42	22
Public transport network length, L_{pt}	[lane-km]	34	25
Average link length of L_{pt} , \bar{l}_{pt}	[km]	0.163	0.279
Share of L_{pt} dedicated to public transport only	[% L_{pt}]	75	60

2.2. Car data

The traffic management system of Zurich operates 4852 traffic detectors at 384 intersections for public transport vehicles, cars, or both (DAV, 2015). Their purpose is to give priority to public transport, support traffic signal control, and identify congestion. In this paper, we concentrate on data from loop detectors that measure car traffic – the loops' geometries do not vary much (around 90% of the loops have a length of 1.5 m and 10% have a length of 3.5 m). Each detector records vehicle counts, q , and occupancy, o , with an accuracy of 0.1 s, aggregated in 15 min intervals. In an internal study, carried out by the city's traffic department, the errors of the loops were determined to be lower than 5% (Birchmeier, 2017). Faulty loops were removed from this data set. All detectors were geo-coded; we collected their exact positions referenced from the next downstream intersection and we attributed them to a lane on a link. Average link length is 160 m in the City center and 280 m in Wiedikon. Most detectors are located close to the next downstream intersection. Thus, the distribution of the relative position of loop detectors with respect to the downstream intersection is not uniform. Therefore, we acknowledge a certain overestimation of the density in the MFD (Ambühl et al., 2017; Buisson and Ladier, 2009; Courbon and Leclercq, 2011). The number of selected loop detectors is 145 in the City center and 68 in Wiedikon.

As density k is not directly measured by loop detectors, its value must be approximated by the space-effective mean length l_e of a car ($k = o/l_e$). For Zurich, this value is around 6.3 m (AKP Verkehrsingenieure, 2016; DAV, 2015). Here, we use the approach from previous empirical studies, e.g., Geroliminis and Daganzo (2008) or Buisson and Ladier (2009), and weight flows and densities by the length l of each link. With the network average flow q_c the total production P_c is given by Eq. (1), and with density k_c the total accumulation N_c is given by Eq. (2). Since not all links are covered by loop detectors, we approximate production and accumulation by scaling flow and density by the total network length L_c . The calculation of the speed in Eq. (3) follows the fundamental relationship.

$$P_c = q_c L_c = \frac{\sum q_i l_i}{\sum l_i} L_c \quad (1)$$

$$N_c = k_c L_c = \frac{\sum k_i l_i}{\sum l_i} L_c \quad (2)$$

$$v_c = \frac{q_c}{k_c} \quad (3)$$

Fig. 2a shows the resulting MFDs from loop detector data for the 5 weekdays, between 06:00 and 24:00 – each data point represents the average of a 15 min interval. Both regions exhibit a similar range of accumulation and production, with Wiedikon having slightly less production. However, when considering average network flows and densities (dividing by the respective network length L_c), we observe a higher capacity in Wiedikon than in the City center and a similar critical density in both regions (not shown in the figure). While Wiedikon shows a decrease in production once the critical accumulation is reached, this congested branch of the MFD is absent for the City center. We assume that this is due to the City center's gating control scheme, designed to reduce congestion during peak hours. Thus, we do not expect strong indications of congestion. Fig. 2b shows the familiar relationship between average speed and accumulation. Wiedikon shows slightly greater free flow speeds than the City center. We attribute this to the differences in intersection density (see Table 1). Wiedikon has on average longer links and fewer intersections than the denser City center, thus, vehicles in Wiedikon need to stop less frequently. Figs. 2a and b show well-defined curves with very little scatter, even though no filter was applied to the data (except for excluding malfunctioning loops). There are multiple reasons for this. First, the investigated regions are rather small. Second, the loop detectors have a high precision (<5% error). Third, the aggregation interval is 15 min, further reducing the scatter. Fourth, in both regions, the number of available routes is very limited and car drivers can rarely change their route to adapt to a traffic situation. Thus, we do not expect to observe large differences in the loading and unloading of the network (Gayah and Daganzo, 2011).

We compute the car passenger accumulation by multiplying the vehicle accumulation by two-hour averages of car passenger occupancy. The latter value is calculated from the trip diary of the Swiss transportation micro-census 2010 (Federal, 2012). We select all car trips heading for any part of Zurich (including both the City center and Wiedikon) and compute the

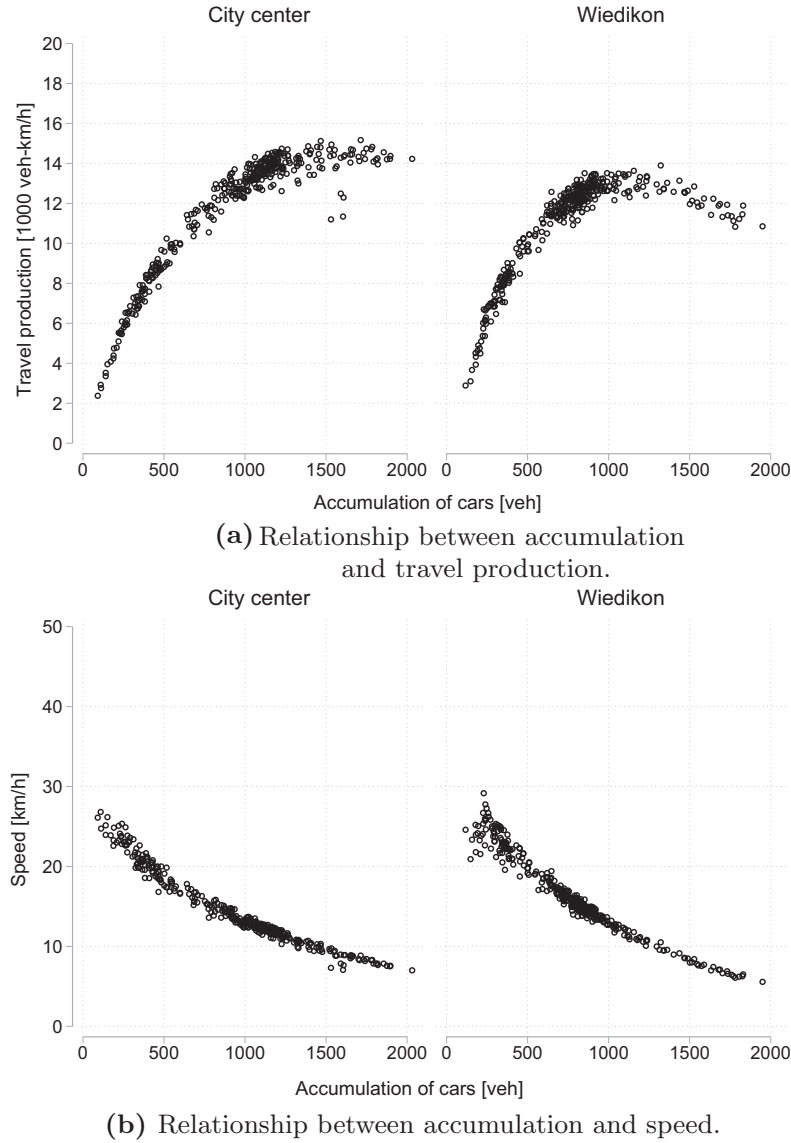


Fig. 2. Fundamental relationships for car traffic in Zurich.

mean car occupancy for weekdays and two-hour intervals, e.g. one value for 06:00 to 08:00, one for 08:00 to 10:00, etc. This makes the calculations of the 3D-pMFD more accurate than taking one single average value over the whole time period. Notice that the average car occupancy during the morning peak is around 1.2 and increases toward the evening to 1.36.

2.3. Public transport data

Data on public transport performance is obtained from Zurich's transit operator, *Verkehrsbetriebe Zürich* (VBZ). The data set contains information on each public transport vehicle's travel time from stop to stop including the dwell time at each stop ([Stadt Zürich, 2016b](#)), recorded by automatic vehicle location (AVL) devices. We add the distance from stop to stop to the dataset.

Passenger occupancies are available for the year 2014 ([Stadt Zürich, 2016a](#)). Generally, the differences between the timetables of 2014 and 2015 are minor and we do not expect significant variation in vehicle occupancies between these two years, given that both data sets represent regular weeks without holidays, and there were no exogenous changes in the city nor the region. We merged both data sets in a flexible way using line number, stop ID, type of day, and a departure time interval of plus/minus five minutes. For example, if in the 2015 speed data set the scheduled departure of a bus is 13:28, we allow for a scheduled departure time window of 13:23–13:33 for the 2014 passenger counts data set.

For each time interval T , the average speed v_{pt} of public transport vehicles is computed according to Eq. (4) using the travel time t_i and the travel distance d_i of each public transport vehicle.

$$v_{pt} = \frac{\sum d_i}{\sum t_i} \quad (4)$$

The accumulation N_{pt} is computed with Eq. (5) and the observation interval T .

$$N_{pt} = \frac{\sum t_i}{T} \quad (5)$$

Then we calculate public transport vehicle production P_{pt} with Eq. (6).

$$P_{pt} = N_{pt} v_{pt} \quad (6)$$

The total passenger accumulation of the public mode is calculated by multiplying the vehicle accumulation by the average vehicle occupancy in each time interval.

3. Empirical 3D-MFD

In this analysis, we focus on the multi-modal interactions and their implications for the speeds of the private and public modes. We aggregate all data points into 15 min intervals to avoid systematic variation in the 3D-MFD, due to the relatively rigid fixed-interval timetable for public transportation in Zurich.

In Fig. 3a we compare the speeds of cars and public transport vehicles during Tuesday, October 27th 2015. Remember that the speeds of public transport vehicles contain the dwell times. In the City center, we observe that the car speeds drop during the morning peak to 11 km/h and during the afternoon peak to 9 km/h, but recover during the course of the day up to 13–14 km/h. The speed of public transport vehicles is around 12 km/h all the time, but shows a slight decrease to around 10 km/h during the afternoon peak. In Wiedikon, speeds of both modes are generally higher than in the City center and show a greater range. In the afternoon, car speeds drop remarkably below public transport speeds.

Fig. 3b shows the total number of travelers in the two regions, stacked by mode. We observe – for both regions – that passenger accumulation increases significantly during morning and evening peaks. In the City center this is mostly captured by public transport, whereas in Wiedikon it is captured by cars. Regarding the share of public transport users, we observe a higher share in the City center than Wiedikon. We attribute this to the higher concentration of public transport lines in the City center (see Table 1).

In Fig. 4, we present the observed 3D-MFDs for the City center and Wiedikon. The horizontal plane represents the accumulation of both modes and the vertical axis the total production. We calculate total production according to Eq. (7). For the reader's convenience we mark the maximum value of the production in each region using a gray plane in Fig. 4.

$$P = P_c + P_{pt} \quad (7)$$

Since this is an empirical data set, the range of observed data points is limited, especially for public transport accumulation (due to the rather constant timetables). That being said, we can still compare the two similarly-sized regions. In general, we register higher public transport accumulation for the City center than for Wiedikon, due to the very high number of public transport lines in the City center, and the longer public transport network.

4. A statistical model for the 3D-MFD based on empirical data

With the available – but limited – range of data, in this section, we quantify the macroscopic relationships using a statistical model. This allows us to use the 3D-MFD in further applications. Fig. 4 shows trends similar to those found in Geroliminis et al. (2014) for the 3D-MFD using simulation data, but our data does not exhibit similar experimental variation because it is empirical. Geroliminis et al. (2014) propose linking car and public transport density with total flow using an exponential function. Both modes' densities enter the argument of the exponential function as a bivariate quadratic function. However, with our data showing limited empirical variation, we cannot estimate this function, especially because extreme values must be arbitrarily defined to fit the curve. Therefore, we follow Zheng and Geroliminis (2016) and define functions for the vehicle based 3D-MFD and the passenger 3D-MFD (3D-pMFD) based on observed data. In the following, we introduce a model based on densities, rather than accumulation, to normalize for the different regions ($k = N/L$).

4.1. 3D-MFD

For simplicity and as a first order approach, we use Greenshields' linear model between density and speed, which has also been applied at the network level (Mahmassani et al., 1987). The speed of public transport v_{pt} is modeled by a linear relationship with car speed v_c , as proposed by Geroliminis et al. (2014) and Zheng and Geroliminis (2013) and covers mode interactions.

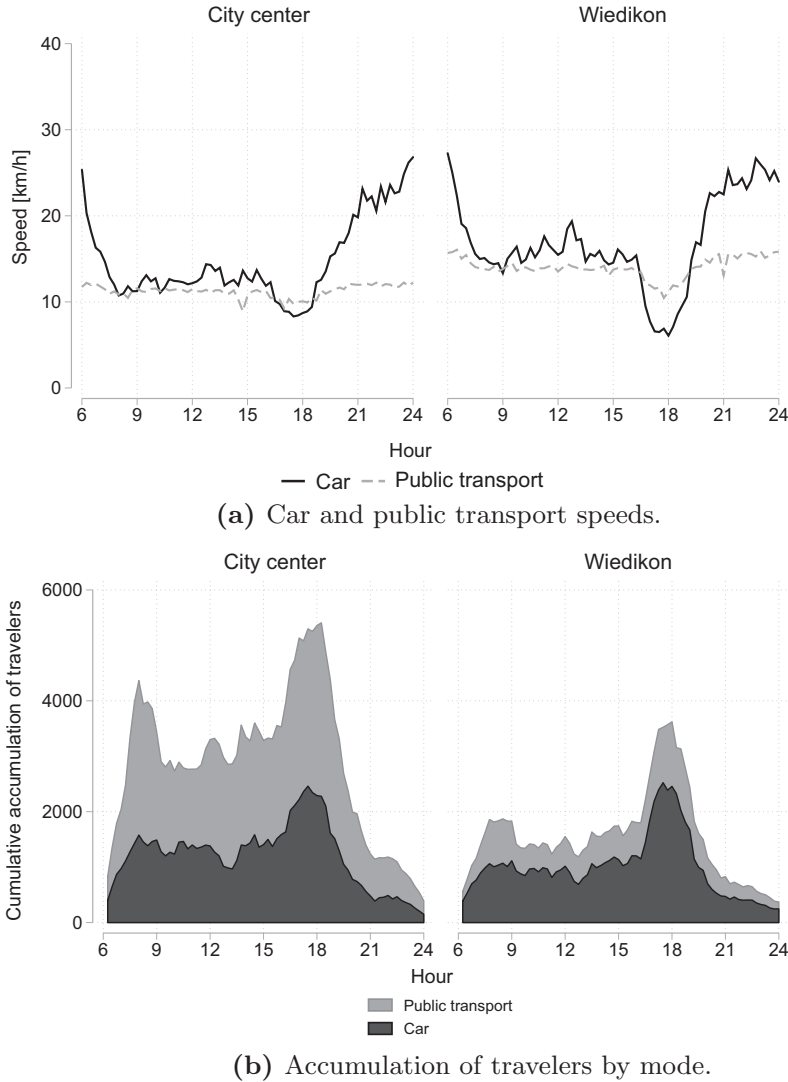


Fig. 3. Bi-modal relationships in the city of Zurich.

Therefore, we propose modeling the 3D-MFD with two equations. The first equation links car speeds v_c to the free flow speed of cars $\beta_{c,0}$, the density of cars k_c , and the density of public transport vehicles k_{pt} . β_c and β_{pt} are coefficients representing the marginal effect of each mode on car speeds.

$$v_c = \beta_{c,0} + \beta_c k_c + \beta_{pt} k_{pt} \quad (8)$$

Using the definition by Geroliminis et al. (2014) and Zheng and Geroliminis (2013), the speed of public transport vehicles v_{pt} is defined in Eq. (9) as a function of car speed v_c . Thus, public transport speed does not explicitly depend on vehicles' densities k_c and k_{pt} . However, v_c is a function of vehicle densities and therefore v_{pt} depends implicitly on vehicle densities. The coefficients to be estimated are $\beta_{pt,0}$ and $\beta_{c,pt}$. $\beta_{c,pt}$ captures the aspect that public transport vehicles typically move slower than cars due to frequent stops, and $\beta_{pt,0}$ adjusts for the fact that public transport speeds might exceed car speeds during congested times due to dedicated lanes. This effect is observed in both regions during the evening peak, see Fig. 3a.

$$v_{pt} = \beta_{c,pt} v_c + \beta_{pt,0} \stackrel{\text{Eq. (8)}}{=} \beta_{c,pt} (\beta_{c,0} + \beta_c k_c + \beta_{pt} k_{pt}) + \beta_{pt,0} \quad (9)$$

4.2. 3D-pMFD

Fig. 5 shows the empirical relation between public transport accumulation of vehicles and passengers. We observe that in reality the public transport operator does not respond linearly to an increase in number of travelers (i.e., with higher number

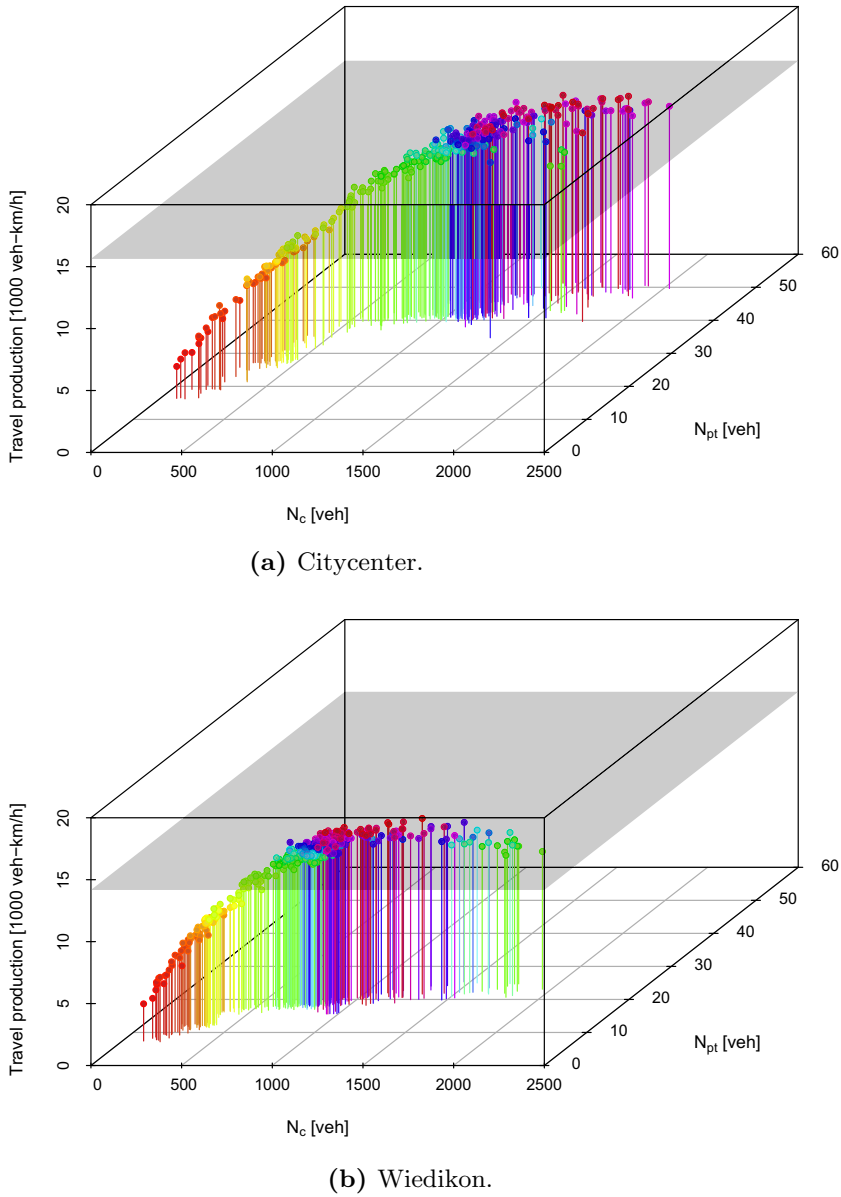


Fig. 4. 3D-MFDs in Zurich. The color progression indicates the total vehicle production progression. The gray plane depicts the maximum production reached. (For interpretation of the references to color in this figure legend, the reader is referred to the web version of this article.)

of public transport passengers, passenger densities in vehicles increase). In the following we try to endogenously capture this phenomenon. The 3D-pMFD is estimated by substituting vehicle densities in Eq. (8) for passenger densities $k_{pax,c}$ for cars and $k_{pax,pt}$ for public transport, as introduced by Chiabaut (2015). Thus, the resulting model equation is changed to Eq. (10). Eq. (9) for public transport vehicle speeds still holds.

$$v_c = \beta_{pax,c,0} + \beta_{pax,c} k_{pax,c} + \beta_{pax,pt} k_{pax,pt} \quad (10)$$

We also use Fig. 5 to convert public transport passenger accumulation to public transport vehicle accumulation. The model used is indicated in the figure. It is clear that the public transport passenger accumulation and public transport vehicle accumulation do not have to remain the same – especially in the long term. In the short time, however, our curve does neither depend on the mode choice nor on the modal split. The clear functional relationship found in Fig. 5 indicates the independence. Note that such trend has its limits, thus we will discuss the model results around the observed ranges of public transport accumulations.

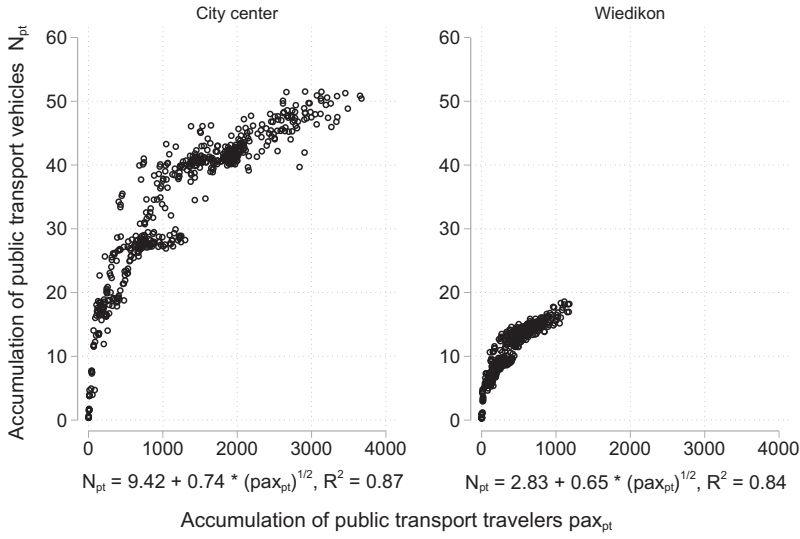


Fig. 5. Capacity provision by the public transport operator for given accumulations of travelers.

5. Model results

5.1. 3D-MFD

This section shows the results of the models defined in the previous section. Using these it is now possible to reconstruct the 3D-MFD and 3D-pMFD (see Fig. 6) by calculating productions with a combination of all observed accumulations. Subsequently, in Section 6 we apply the 3D-pMFD to discuss the optimal allocation of travelers to each mode.

In Table 2 we show the model results for the vehicle 3D-MFD for both regions in Zurich, based on the data set described in Section 2 (5 weekdays, 06:00–24:00, 15 min intervals; total 360 observations). The model was estimated using ordinary least squares (OLS). All estimates are significant and show the expected signs. Wiedikon shows a slightly higher free flow speed than the City center and a marginal effect of car density in the same order of magnitude; both findings are in accordance with the results from Fig. 2b. The higher free flow speed can be attributed to longer links and fewer signalized intersections in Wiedikon (see Table 1). Comparing the marginal effects of public transport vehicles, we find a decrease in speeds of 5.7 km/h per additional public transport density of 1 veh/km in the City center whereas this decrease amounts to 6.7 km/h in Wiedikon. At a density of one public transport vehicle per kilometer, the elasticity of public transport vehicles on car speeds in the City center is -0.4 and in Wiedikon -0.7 . We expect that the lower impact of public transport vehicles in the City center is due to the larger share of dedicated lanes. Considering public transport speeds, we observe 10.8 km/h in Wiedikon and 9.6 km/h in the City center for the constant $\beta_{pt,0}$ and around 0.12 km/h change in public transport speeds for 1 km/h change in car speed in the City center and 0.2 km/h in Wiedikon. These findings are in line with Fig. 3a.

5.2. 3D-pMFD

For the 3D-pMFD, Table 3 presents the model estimates. All model estimates show the expected signs and are significantly different from zero. Compared to the vehicle 3D-MFD estimates, differences in the magnitude of effects of the 3D-pMFD reflect the different vehicle occupancies. Note that the estimates for the public transport speed are identical because the model equation has not changed. The model estimates for the car speed equations emphasize that one additional passenger does, at least, impose one order of magnitude less impact on all car drivers when he chooses public transport instead of the car. In the City center, this ratio is even stronger than in Wiedikon, arguably, again, due to the larger share of dedicated lanes in the City center than in Wiedikon.

5.3. Predicted 3D-MFD

Using the estimates from Table 2, we now predict the 3D-MFD shape for both regions in Figs. 6a and b. Speeds \hat{v}_c and \hat{v}_{pt} are calculated over a range of accumulations N_c and N_{pt} . Thus, we calculate the total production with Eq. (7). The 3D-pMFDs in Figs. 6c and d are based on estimates from Table 3 and use the total passenger production according to Eq. (7). Additionally, we use the model from Fig. 5 to estimate the number of public transport vehicles per public transport passenger accumulation. For the car occupancy we use a constant value of 1.36 pax/veh. Thus, the 3D-pMFD we present here is a representation of the reality as of today – using the same public transport service levels for the same public transport

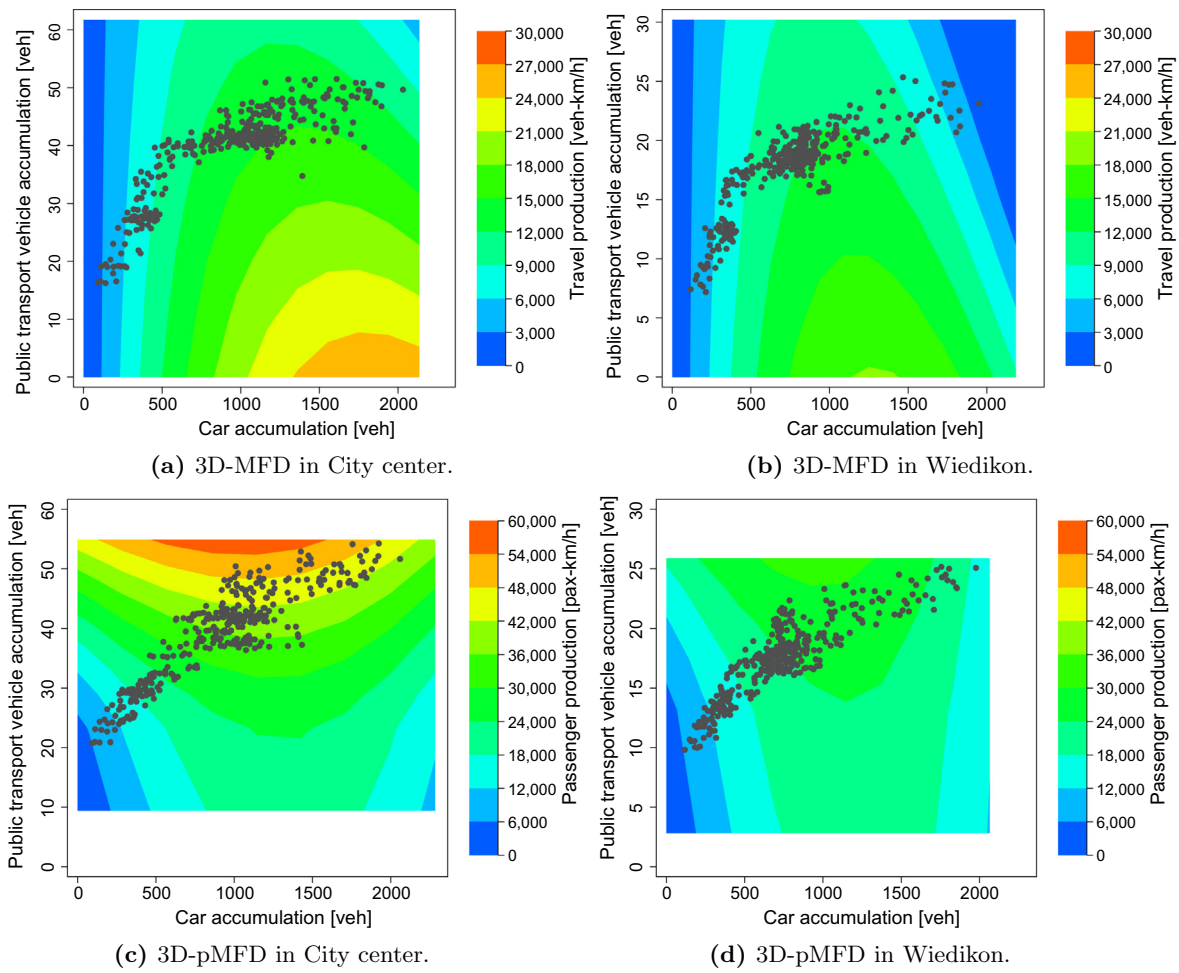


Fig. 6. Predicted 3D-MFD shape for passenger and vehicles. The gray dots represent the range of empirical observations.

Table 2

Model estimates for the 3D-MFD. The dependent variables are the space-mean speeds of cars and public transport vehicles. All estimates are significant at 1% level of significance.

	City center		Wiedikon	
	Car	Public transport	Car	Public transport
Car density [veh/km]	-0.288		-0.345	
Public transport vehicle density [veh/km]	-5.659		-6.726	
Car speed [km/h]		0.116		0.197
Constant	27.933	9.574	28.448	10.794
R ²	0.96	0.49	0.94	0.79
N	360	360	360	360

passenger accumulations. For the reader's convenience we add the top-down view of Fig. 4 to Fig. 6 to see the range of car and public transport vehicle accumulations for which data is available.

It is clear that our predicted MFDs provide higher accuracies for points closer to, or within the region of the empirical data. Any extrapolation of our model beyond the observed range of data should be considered with caution. Nevertheless, our model has a strong indicative character and gives a first empirical insight regarding the interactions of multi-modal traffic at a network level. The model is intuitive and when we compare the results of our extrapolated 3D-MFD and 3D-pMFD with the ones from simulations, such as the one from San Francisco, estimated by Geroliminis et al. (2014), we see similar trends. Both, the simulation and our prediction model show concave curves with a maximum vehicular production for zero public transport accumulation, and a similar skewness. In contrast, passenger production increases with greater

Table 3

Model estimates for the passenger 3D-pMFD. The dependent variables are the space-mean speeds of cars and public transport vehicles. All estimates are significant at 1% level of significance.

	City center		Wiedikon	
	Car	Public transport	Car	Public transport
Car passenger density [pax/km]	-0.252		-0.240	
Public transport passenger density [pax/km]	-0.022		-0.076	
Car speed [km/h]		0.116		0.197
Constant	23.480	9.574	25.797	10.794
R ²	0.89	0.49	0.90	0.79
N	360	360	360	360

accumulation of public transport vehicles; the maximum passenger production is outside the range of observed accumulations. Arguably, the curves' shapes are mainly determined by the functional form of the model.

Additionally, we can compare the rate at which the critical accumulation (the vehicle accumulation which maximizes travel production) changes. We see that additional public transport vehicles decrease the critical car accumulation. The rate at which the critical car accumulation decreases with increasing public transport vehicle accumulation indicates the level of interaction between the two modes. For the City center one additional public transport vehicle decreases the critical car accumulation by around 12 cars, whereas in Wiedikon this number is 10. Note that these values are not directly comparable with the interaction effects estimated in Table 2.

6. Optimal share of public transport users based on the 3D-pMFD

This section presents a new application of the 3D-pMFD. Previous applications of the 3D-MFD focused on control algorithms. For example, [Zheng and Geroliminis \(2013\)](#) dynamically allocated space to buses, depending on the total passenger demand and including congestion pricing. [Chiabaut \(2015\)](#) showed that the passenger MFD can be used to evaluate control strategies, and proposed a conceptual control strategy for optimal bus headways. Similar to [Chiabaut \(2015\)](#), here we propose an evaluation framework based on the results presented in previous sections. However, instead of concentrating on passenger flows, we apply the 3D-pMFD to compute and compare journey speeds of car users v_c and public transport users v_{pt} of a given population of travelers (excluding users' access time). This idea traces back to the work by [Smeed \(1968\)](#), where the average journey time is related to the number of commuters, which is further split into bus and car passengers. The results do not lead directly to any control algorithms, but can inform different policies regarding multi-modal operations. Along these lines, we define the weighted average journey speed \bar{v} of car passengers pax_c and public transport passengers pax_{pt} in Eq. (11). We then plot the results in Fig. 7 as a function of the share of public transport users $pax_{pt}/(pax_c + pax_{pt})$ for a given total passenger accumulation $pax_{tot} = k_{pax,c}L_c + k_{pax,pt}L_{pt} = pax_c + pax_{pt}$.

$$\bar{v} = \frac{v_{pt}pax_{pt} + v_c pax_c}{pax_{tot}} \quad (11)$$

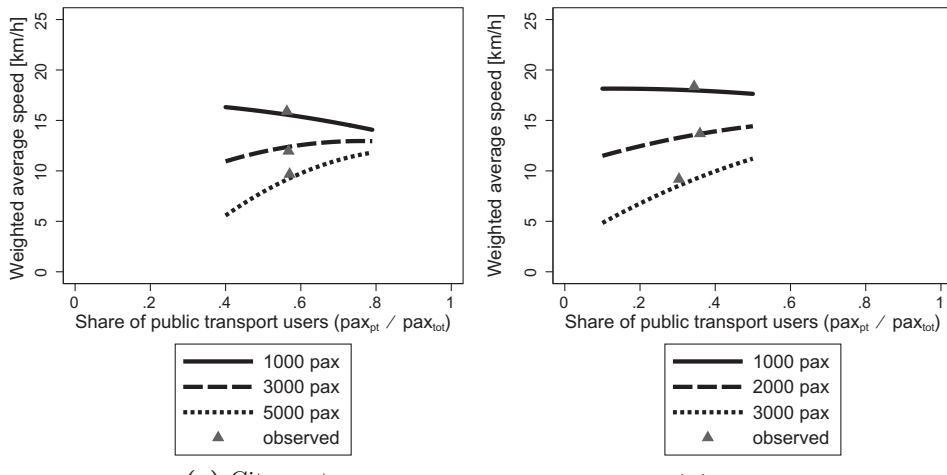


Fig. 7. Share of public transport passengers and average journey speeds in Zurich.

This can be seen as a supply function of the infrastructure's capacity, i.e. which travel times can be reached given a certain infrastructure and the capacity provision of the public transport operation as shown in Fig. 5. We show the relationship between share of public transport users and weighted average journey speed for three different passenger accumulation levels. 5000 pax for the City center and 3000 pax for Wiedikon represent the average accumulations during peak hour traffic. The share of public transport users maximizing the weighted average journey speed can be seen as an optimal share from the infrastructure capacity perspective. Note that we only plot realistic shares around plus/minus 20 percentage points of the observed share of public transport users. We observe a similar pattern in both regions as long as the total passenger accumulation exceeds certain minimum threshold: when the number of passengers increases, a larger number must use public transport to increase the weighted average journey speed in the network. The higher the level of passenger accumulation, the more the network benefits from shifting its users to using public transport. Conversely, for relatively low passenger accumulations (1000 pax), the weighted average speed remains stable or even decreases when more travelers use the public transport services.

Furthermore, we include the observed points for the three different levels of passenger accumulation. These observed values are shown as a triangle in Fig. 7. They give an insight on how well the existing passenger accumulation is distributed across the two modes. We see that the City center already has a high share of public transport users, which leads to a speed close to the optimum for a medium-level passenger accumulation. For higher levels of passenger accumulation, the weighted average speed would benefit from an increasing share of public transport users.

Note that the 3D-pMFD estimates do not capture the decrease in waiting, transfer and thus travel times if the operator increases the number of vehicles. Consequently, the experienced journey speeds of public transport travelers in the network are expected to be higher than those presented here. Additionally, the estimated 3D-pMFD describes the observed dynamics during the week in October 2015.

7. Conclusions

This paper presents the first empirical 3D-MFD for vehicles and passengers, for two regions in Zurich. The 3D-MFDs are estimated based on loop detector data, AVL trajectories of public transport vehicles, and vehicle occupancies (i.e., number of passengers per vehicle). We use a linear model between the vehicle densities and car speeds and a linear model between public transport and car speeds. We observe negative marginal effects for every additional vehicle (either public transport or car) on the average car speed – this is in line with previous studies (Geroliminis et al., 2014; Smeed, 1961, 1968). The marginal effect of one public transport vehicle is more than ten times greater than the marginal effect of a car. At a density of one public transport vehicle per kilometer, the elasticity of public transport vehicles on car speeds in the City center is -0.4 and in Wiedikon -0.7 . We attribute these differences in the two regions to the higher share of dedicated public transport lanes in the City center. Even though both regions have already high shares of dedicated lanes for public transport, it is important to note that other, substantial interactions are present, especially at intersections. This effect is amplified in Zurich, since the public transport prioritization scheme gives high priority to public transport (Ambühl et al., 2017).

We introduce a novel application of the 3D-pMFD, discussing an optimal share of public transport users. We emphasize that starting from a certain level of passenger accumulation, the provision of public transport is necessary to improve urban speeds. With the 3D-MFD, policy makers and transport planners can assess policy changes at vehicle and passenger level for both modes. In essence, a comparison between the observed and the optimal share of public transport users gives quantitative insights on how efficiently a city's multi-modal transportation network operates. Authorities can then formulate changes necessary to shift the network to its optimum directly from a 3D-pMFD. Recall that the policy-relevant implications should be carefully evaluated because of limited variance and range in the data. However, most applications building on – and around – the 3D-MFD and the 3D-pMFD will be based on the observed equilibrium. For such small deviations around the observed 3D-MFD, our estimates are appropriate.

This study does have some data limitations. Overall, the limited exogenous empirical variation in public transport due to rather constant timetables limits the validity of the model estimates to the observed range and does not allow estimation of second order effects. As the timetable and public transport routes cannot be changed 'ad libitum', it is not possible to achieve larger experimental variation. We emphasize that our model is conceptual and gives appropriate results for the observed range of empirical data, but indicative results otherwise. Nevertheless, the sign and the magnitude of the estimated coefficients are helpful to indicate how strongly one additional public transport vehicle per km or one additional car per km influences overall speeds. Furthermore, complete car data is not available for all links of the entire road network. This implies that our 3D-MFD might be biased due to an unrepresentative sample, but as the share of covered network length is large, we expect this bias to be small. Moreover, some assumptions are made about the space-mean effective length of a vehicle, which might only hold approximately, and the distribution of the loop detectors within the length of the links might have an impact on the representativeness of the results. The sample is aggregated to 15 min intervals, thereby avoiding random scattering caused by the public transport timetable when considering smaller intervals. These greater intervals, in turn, reduce the sample size for the model estimation. Lastly, the passenger occupancies are not observed during the same time period as the loop detector and public transport data set, but are taken from previous years. However, given the lack of exogenous changes, we do not expect large variations between 2015 and previous years.

Regarding our formulation of the 3D-pMFD and the public transport vehicle provision, it is clear that such a provision cannot follow this trend for all levels of public transport passengers. However, around public transport passenger levels

which are observed in reality and for a short term perspective, this public transport provision function is appropriate. It is also important to note that the 3D-pMFD shown in this paper depicts the observed situation. If, however, we were interested in the theoretically possible maximum passenger flow, then the public transport passenger occupancy should be held constant at the maximum allowed passenger occupancy, and at the same time, car occupancies should also be set to the maximum passengers allowed per car.

Our future research will concentrate on analytical approximations of the 3D-MFD following the work by [Boyaci and Geroliminis \(2011\)](#), [Chiabaut \(2015\)](#), [Daganzo and Geroliminis \(2008\)](#), [Geroliminis and Boyaci \(2012\)](#) and [Leclercq and Geroliminis \(2013\)](#). This kind of work would not only improve general understanding of the 3D-MFD, but would also allow derivation of a methodology to estimate the 3D-MFD with less data, based on infrastructure and public transport system parameters.

Acknowledgments

This work was supported by ETH Research Grants ETH-04 15-1 and ETH-27 16-1. We would like to thank the City of Zurich for providing loop detector and public transport data. The authors acknowledge the helpful comments of Nan Zheng, Martin Fellendorf, Markus Friedrich and Hani S. Mahmassani on earlier versions of the paper. This paper also benefited from the very insightful comments of the anonymous referees.

References

- [Aboudolas, K., Geroliminis, N., 2013. Perimeter and boundary flow control in multi-reservoir heterogeneous networks. *Transport. Res. Part B: Methodol.* 55, 265–281.](#)
- [Adler, M.W., van Ommeren, J.N., 2016. Does public transit reduce car travel externalities? Quasi-natural experiments' evidence from transit strikes. *J. Urban Econ.* 92, 106–119.](#)
- [AKP Verkehrsingenieure AG, 2016. Forschungsprojekt VSS 2011/203 Geometrie des Fahrzeugparks der Schweiz.](#)
- [Ambühl, L., Loder, A., Menendez, M., Axhausen, K.W., 2017. Empirical macroscopic fundamental diagrams: new insights from loop detector and floating car data. Paper presented at the 96th Annual Meeting of the Transportation Research Board, Washington, D.C.](#)
- [Ambühl, L., Menendez, M., 2016. Data fusion algorithm for macroscopic fundamental diagram estimation. *Transport. Res. Part C: Emerg. Technol.* 71, 184–197.](#)
- [Anderhub, G., Dorbritz, R., Weidmann, U., 2008. Leistungsfähigkeitsbestimmung öffentlicher Verkehrssysteme. Schriftenreihe 139. IVT, ETH Zürich. Zürich.](#)
- [Anderson, M.L., 2014. Subways, strikes, and slowdowns: the impacts of public transit on traffic congestion. *Am. Econ. Rev.* 104, 2763–2796.](#)
- [Arnet, K., Guler, S.I., Menendez, M., 2015. Effects of multimodal operations on urban roadways. *Transport. Res. Rec.: J. Transport. Res. Board* 2533, 1–7.](#)
- [Birchmeier, U., 2017. Verification of Traffic Light Detectors. Internal Document. Dienstabteilung Verkehr, Stadt Zürich.](#)
- [Boyaci, B., Geroliminis, N., 2011. Estimation of the network capacity for multimodal urban systems. *Proc. – Soc. Behav. Sci.* 16, 803–813.](#)
- [Buisson, C., Ladier, C., 2009. Exploring the impact of homogeneity of traffic measurements on the existence of macroscopic fundamental diagrams. *Transport. Res. Rec.: J. Transport. Res. Board* 2124, 127–136. <http://dx.doi.org/10.3141/2124-12>.](#)
- [Cao, J., Menendez, M., 2015. System dynamics of urban traffic based on its parking-related-states. *Transport. Res. Part B: Methodol.* 81, 718–736.](#)
- [Chatman, D.G., Noland, R.B., 2011. Do public transport improvements increase agglomeration economies? A review of literature and an agenda for research. *Transp. Rev.* 31, 725–742.](#)
- [Chiabaut, N., 2015. Evaluation of a multimodal urban arterial: the passenger macroscopic fundamental diagram. *Transport. Res. Part B: Methodol.* 81, 410–420.](#)
- [Chiabaut, N., Xie, X., Leclercq, L., 2014. Performance analysis for different designs of a multimodal urban arterial. *Transportmetrica B: Transp. Dyn.* 2, 229–245.](#)
- [Courbon, T., Leclercq, L., 2011. Cross-comparison of macroscopic fundamental diagram estimation methods. *Proc. – Soc. Behav. Sci.* 20, 417–426.](#)
- [Daganzo, C.F., 2007. Urban gridlock: macroscopic modeling and mitigation approaches. *Transport. Res. Part B: Methodol.* 41, 49–62. <http://dx.doi.org/10.1016/j.trb.2006.03.001>.](#)
- [Daganzo, C.F., Geroliminis, N., 2008. An analytical approximation for the macroscopic fundamental diagram of urban traffic. *Transport. Res. Part B: Methodol.* 42, 771–781.](#)
- [DAV, 2015. Loop Detector Data in Zurich. Stadt Zürich – Dienstabteilung Verkehr \(DAV\).](#)
- [Du, J., Rakha, H., Gayah, V.V., 2016. Deriving macroscopic fundamental diagrams from probe data: issues and proposed solutions. *Transport. Res. Part C: Emerg. Technol.* 66, 136–149.](#)
- [Gayah, V.V., Daganzo, C.F., 2011. Clockwise hysteresis loops in the macroscopic fundamental diagram: an effect of network instability. *Transport. Res. Part B: Methodol.* 45, 643–655. <http://dx.doi.org/10.1016/j.trb.2010.11.006>.](#)
- [Geroliminis, N., 2015. Cruising-for-parking in congested cities with an MFD representation. *Econ. Transport.* 4, 156–165.](#)
- [Geroliminis, N., Boyaci, B., 2012. The effect of variability of urban systems characteristics in the network capacity. *Transport. Res. Part B: Methodol.* 46, 1607–1623.](#)
- [Geroliminis, N., Daganzo, C.F., 2008. Existence of urban-scale macroscopic fundamental diagrams: some experimental findings. *Transport. Res. Part B: Methodol.* 42, 759–770.](#)
- [Geroliminis, N., Zheng, N., Ampountolas, K., 2014. A three-dimensional macroscopic fundamental diagram for mixed bi-modal urban networks. *Transport. Res. Part C: Emerg. Technol.* 42, 168–181.](#)
- [Girault, J.T., Gayah, V.V., Guler, I., Menendez, M., 2016. Exploratory analysis of signal coordination impacts on macroscopic fundamental diagram. *Transport. Res. Rec.: J. Transport. Res. Board* 2560, 36–46. <http://dx.doi.org/10.3141/2560-05>.](#)
- [Godfrey, J.W., 1969. The mechanism of a road network. *Traffic Eng. Contr.* 11, 323–327.](#)
- [Gronau, R., 2000. Optimum diversity in the public transport market. *J. Transp. Econ. Policy* 34, 21–41.](#)
- [Gu, W., Cassidy, M.J., Gayah, V.V., Ouyang, Y., 2013. Mitigating negative impacts of near-side bus stops on cars. *Transport. Res. Part B: Methodol.* 47, 42–56. <http://dx.doi.org/10.1016/j.trb.2012.09.005>.](#)
- [Gu, W., Gayah, V.V., Cassidy, M.J., Saade, N., 2014. On the impacts of bus stops near signalized intersections: models of car and bus delays. *Transport. Res. Part B: Methodol.* 68, 123–140. <http://dx.doi.org/10.1016/j.trb.2014.06.001>.](#)
- [Guler, S., Menendez, M., 2014a. Analytical formulation and empirical evaluation of pre-signals for bus priority. *Transport. Res. Part B: Methodol.* 64, 41–53. <http://dx.doi.org/10.1016/j.trb.2014.03.004>.](#)
- [Guler, S., Menendez, M., 2014b. Evaluation of presignals at oversaturated signalized intersections. *Transport. Res. Rec.: J. Transport. Res. Board* 2418, 11–19. <http://dx.doi.org/10.3141/2418-02>.](#)
- [Haddad, J., Geroliminis, N., 2012. On the stability of traffic perimeter control in two-region urban cities. *Transport. Res. Part B: Methodol.* 46, 1159–1176.](#)

- He, H., Guler, S.I., Menendez, M., 2016. Adaptive control algorithm to provide bus priority with a pre-signal. *Transport. Res. Part C: Emerg. Technol.* 64, 28–44. <http://dx.doi.org/10.1016/j.trc.2016.01.009>.
- He, H., Menendez, M., Guler, S.I., 2017. Analytical evaluation of flexible sharing strategies on multi-modal arterials. In: International Symposium on Traffic and Transportation Theory, ISTTT, 2017.
- Hensher, D.A., 2001. Measurement of the valuation of travel time savings. *J. Transp. Econ. Policy* 35, 71–98.
- Herman, R., Prigogine, I., 1979. A two-fluid approach to town traffic. *Science* 204, 148–151.
- Ji, Y., Luo, J., Geroliminis, N., 2014. Empirical observations of congestion propagation and dynamic partitioning with probe data for large-scale systems. *Transport. Res. Rec.: J. Transport. Res. Board* 2422, 1–11.
- Knoop, V.L., de Jong, D., Hoogendoorn, S., 2014. The influence of the road layout on the network fundamental diagram. Paper presented at the 93rd Annual Meeting of the Transportation Research Board, Washington, D.C..
- Knoop, V.L., van Lint, H., Hoogendoorn, S.P., 2015. Traffic dynamics: its impact on the macroscopic fundamental diagram. *Phys. A: Stat. Mech. Appl.* 438, 236–250.
- Köhler, U., Strauss, S., Wichmann, S., 1998. Berichte der Bundesanstalt für Straßenwesen. Verkehrstechnik 57. Wirtschaftsverlag NW. Bremerhaven.
- Laval, J.A., Castrillón, F., 2015. Stochastic approximations for the macroscopic fundamental diagram of urban networks. *Transport. Res. Proc.* 7, 615–630. <http://dx.doi.org/10.1016/j.trpro.2015.06.032>.
- Leclercq, L., Geroliminis, N., 2013. Estimating MFDs in simple networks with route choice. *Transport. Res. Part B: Methodol.* 57, 468–484.
- Leclercq, L., Sénécat, A., Mariotte, G., 2017. Dynamic macroscopic simulation of on-street parking search: a trip-based approach. *Transport. Res. Part B: Methodol.* 101, 268–282. <http://dx.doi.org/10.1016/j.trb.2017.04.004>.
- Lüthy, N., Guler, S.I., Menendez, M., 2016. Systemwide effects of bus stops: bus bays vs. curbside bus stops. Paper presented at the 95th Annual Meeting of the Transportation Research Board, Washington, D.C..
- Mahmassani, H., Williams, J.C., Herman, R., 1984. Investigation of network-level traffic flow relationships: some simulation results. *Transport. Res. Rec.: J. Transport. Res. Board* 971, 121–130.
- Mahmassani, H., Williams, J.C., Herman, R., 1987. Performance of urban traffic networks. In: Gartner, N., Wilson, N.H.M. (Eds.), *Proceedings of the 10th International Symposium on Transportation and Traffic Theory*. Elsevier Science Publishing, pp. 1–20.
- Menendez, M., Ortigosa, J., Ambühl, L., Axhausen, K.W., Ciari, F., Bösch, P.M., Geroliminis, N., Zheng, N., 2016. NetCap: Intermodale Strecken-/Linien- und Netzleistungsfähigkeit, Schlussbericht SVI 2004/032. Schriftenreihe 1563. IVT ETH Zürich und LUTS EPF Lausanne.
- Moghimiadari, S., Furth, P.G., Cesme, B., 2016. Predictive tentative transit signal priority with self-organizing traffic signal control. *Transport. Res. Rec.: J. Transport. Res. Board* 2557, 77–85. <http://dx.doi.org/10.3141/2557-08>.
- Muhlich, N., Gayah, V.V., Menendez, M., 2015. An examination of MFD hysteresis patterns for hierarchical urban street networks using micro-simulation. *Transport. Res. Rec.: J. Transport. Res. Board* 2491, 117–126.
- Nikias, V., Guler, S.I., Menendez, M., 2016. Effects of bus operations on the traffic capacity of urban networks: a simulation study, in: Paper presented at the 95th Annual Meeting of the Transportation Research Board, Washington, D.C..
- Ortigosa, J., Gayah, V., Menendez, M., 2017a. Analysis of one-way and two-way street configurations on urban grid networks. *Transportmetrica B: Transp. Dyn.* (in press). <http://dx.doi.org/10.1080/21680566.2017.1337528>.
- Ortigosa, J., Menendez, M., Gayah, V.V., 2015. Analysis of network exit functions for various urban grid network configurations. *Transport. Res. Rec.: J. Transport. Res. Board* 2491, 12–21.
- Ortigosa, J., Zheng, N., Menendez, M., Geroliminis, N., 2017b. Analysis of the 3D-vMFDs of the urban networks of Zurich and San Francisco. Paper presented at the 96th Annual Meeting of the Transportation Research Board, Washington, D.C..
- Schreiber, A., Loder, A., Axhausen, K.W., 2016. Urban mode and subscription choice – an application of the three-dimensional MFD. Paper presented at the 16th Swiss Transport Research Conference, Ascona, May 2016.
- Small, K.A., Verhoef, E.T., 2007. *The Economics of Urban Transportation*. Routledge, Abingdon.
- Smeed, R.J., 1961. The Traffic Problem in Towns. Statistical Society, Manchester.
- Smeed, R.J., 1968. Traffic studies and urban congestion. *J. Transp. Econ. Policy* 2, 33–70.
- Stadt Zürich, 2016a. Fahrgästzahlen VBZ. Stadt Zürich Open Data. URL: <<https://data.stadt-zuerich.ch/dataset/vbz-fahrgastzahlen-ogg>>.
- Stadt Zürich, 2016b. Fahrzeiten der VBZ im Soll-Ist-Vergleich. Stadt Zürich Open Data. URL: <<https://data.stadt-zuerich.ch/dataset/vbz-fahrzeiten-ogg>>.
- Swiss Federal Statistical Office (BFS), 2012. Mobilität in der Schweiz – Ergebnisse des Mikrozensus Mobilität und Verkehr 2010. Swiss Federal Statistical Office (BFS), Neuchatel.
- Thomson, J., 1967. Speeds and flows of traffic in central London: 2. Speed-flow relations. *Traffic Eng. Contr.* 8, 721–725.
- Tirachini, A., Hensher, D.A., 2012. Multimodal transport pricing: first best, second best and extensions to non-motorized transport. *Transp. Rev.* 32, 181–202.
- Tsubota, T., Bhaskar, A., Chung, E., 2014. Macroscopic fundamental diagram for Brisbane, Australia: empirical findings on network partitioning and incident detection. *Transport. Res. Rec.: J. Transport. Res. Board* 2421, 12–21.
- Wang, P.F., Wada, K., Akamatsu, T., Hara, Y., 2015. An empirical analysis of macroscopic fundamental diagrams for Sendai road networks. *Interdiscipl. Inform. Sci.* 21, 49–61.
- Wardrop, J., 1968. Journey speed and flow in central urban areas. *Traffic Eng. Contr.* 9, 528–532.
- Williams, J.C., Mahmassani, H.S., Iani, S., Herman, R., 1987. Urban traffic network flow models. *Transport. Res. Rec.: J. Transport. Res. Board* 1112, 78–88.
- Zheng, N., Geroliminis, N., 2013. On the distribution of urban road space for multimodal congested networks. *Transport. Res. Part B: Methodol.* 57, 326–341.
- Zheng, N., Geroliminis, N., 2016. Modeling and optimization of multimodal urban networks with limited parking and dynamic pricing. *Transport. Res. Part B: Methodol.* 83, 36–58.
- Zheng, N., Rérat, G., Geroliminis, N., 2016. Time-dependent area-based pricing for multimodal systems with heterogeneous users in an agent-based environment. *Transport. Res. Part C: Emerg. Technol.* 62, 133–148.
- Zheng, N., Waraich, R.A., Axhausen, K.W., Geroliminis, N., 2012. A dynamic cordon pricing scheme combining a macroscopic and an agent-based traffic model. *Transport. Res. Part A: Policy Pract.* 46, 1291–1303.